Does Surface Structure of Oxide Affect Strong Metal-Support Interaction with Pt? Pt on Fe_3O_4(001) vs Fe_3O_4(111).

Ke Zhang, Shamil Shaikhutdinov,* Hans-Joachim Freund

Abteilung Chemische Physik, Fritz-Haber-Institut der Max-Planck-Gesellschaft, Faradayweg 4-6, 14195 Berlin, Germany

Abstract.

We studied the structure and thermal stability of Pt deposited on a Fe_3O_4(001) thin film to make a comparison with the Pt/Fe_3O_4(111) system showing a strong metal-support interaction (SMSI) via encapsulation. Pt ad-atoms strongly interact with the (√2×√2)R45° reconstructed Fe_3O_4(001) surface and adsorb monoatomically on the "narrow" sites. Metal sintering sets in only above 700 K, resulting in cuboid Pt nanoparticles exposing primarily (100) and (110) facets. Concomitantly, CO adsorption on Pt is fully suppressed as a result of SMSI. The results provided strong evidence that the Pt nanoparticles on Fe_3O_4(001) are encapsulated by an FeO(111) layer in the same manner as observed for hemispherical Pt particles on Fe_3O_4(111). The comparison suggests that the SMSI effect via encapsulation is insensitive to the surface structure of oxide, although the latter strongly affects the particle morphology.

Keywords: strong metal-support interaction • surface structures • Pt catalysts • thin films

* Corresponding author. E-mail: shaikhutdinov@fhi-berlin.mpg.de

Introduction

Strong metal-support interaction (SMSI),[1] often observed for metal particles supported on reducible oxides, is mostly discussed in terms of encapsulation of the metal by the oxide.[2] Although the encapsulation may, to some extent, be rationalized on thermodynamic grounds using surface energy considerations, an atomic description of how a metal particle becomes covered by an oxide is still missing. Another interesting yet poorly studied issue is whether the SMSI effects are structure sensitive, i.e. dependent on the surface structure of the oxide support. Indeed, the interaction primarily depends on the adhesion energy between the metal and the oxide, which is envisioned to depend on the interface structure. To gain a fundamental understanding of the SMSI effects, model studies are carried out, in which metal nanoparticles are deposited in a controllable manner on well-defined oxide surfaces in the form of single crystals or thin films.[3] In particular, previous studies on Pd/TiO_2(110)[4] and Pt/Fe_3O_4(111)[5] indicated that the encapsulation proceeds via mass transport along the surface rather than through the metal particle.

With respect to iron oxides as a typical reducible oxide support, model studies were primarily focused on the Fe_3O_4(111) surface.[6] In particular, our own studies on metal (Au, Pd, Pt) deposited on Fe_3O_4(111) thin films showed the formation of hemi-spherical nanoparticles exposing (111) top facets.[3b, 7] To date, only Pt was found to exhibit the SMSI effect via encapsulation by a FeO(111) single layer.[5, 8] Recently, more work has been directed toward the Fe_3O_4(001) surface following expectations of a large difference in reactivity when compared to the (111) surface (see, for example, ref. [9]).

High-resolution scanning tunneling microscopy (STM) studies of Au,[10] Pd[11] and Ag[12] on the well-defined (√2×√2)R45° reconstructed surfaces of Fe_3O_4(001) showed strong interaction and remarkable thermal stability of the metal ad-atoms. High energy electron diffraction, transmission electron microscopy, and atomic force microscopy studies of Pt, Au and Ag films of a few nanometers in thickness on a Fe_3O_4(001) substrate revealed certain epitaxial relationships between the metal and iron oxide depending both on the nature of the metals and the deposition temperature (470 – 1000 K).[13] The authors concluded that among the metals studied, Pt is the metal for which the adhesion energy to Fe_3O_4 is the highest, despite having the largest mismatch between the lattice constants when compared

to Ag and Au. (Note, however, that the surface termination of the Fe_3O_4(001) films grown on MgO(001) used in this study was not determined).

Magnetite Fe_3O_4 has an inverse spinel structure. It is generally accepted that the Fe_3O_4(111) surface is terminated by tetrahedrally-coordinated Fe atoms over the close-packed oxygen layer (Fig. 1a), although it critically depends on the preparation conditions.[6d, 14] In the <001> direction, the so-called "B-layer" termination, consisting of the mixed octahedrally coordinated iron and oxygen atoms seems to be the most stable over a broad range of oxygen pressures as predicted by density functional theory (DFT) (Fig. 1b).[15] Although it is well documented that the Fe_3O_4(001) surface exhibits a (√2×√2)R45° reconstruction, its atomic structure remains controversial. Very recently, on the basis of quantitative low-energy electron diffraction (LEED) and STM studies combined with DFT calculations, the reconstruction has been rationalized in terms of an ordered array of subsurface iron vacancies and interstitials.[16]

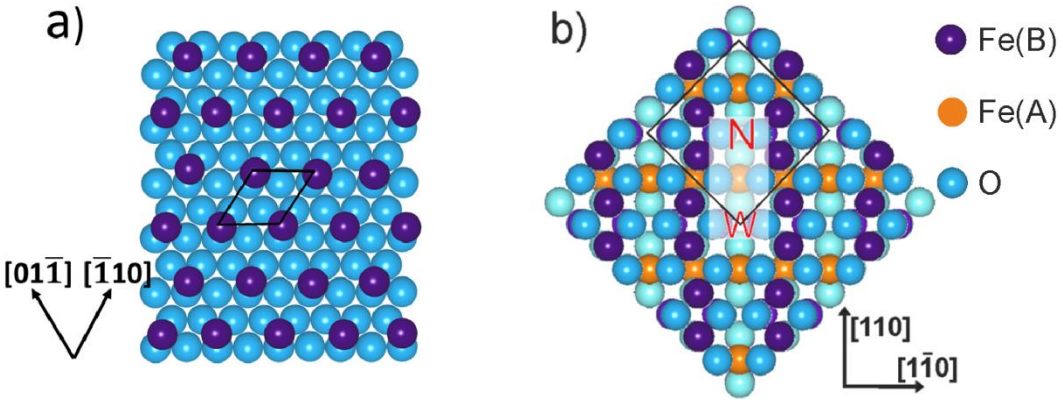

Figure 1. Top views and the units cells of the Fe_3O_4(111) (a) and (√2×√2)R45°-reconstructed Fe_3O_4(001) (b) surfaces. The wide (W) and narrow (N) sites in the (√2×√2)R45°-Fe_3O_4(001) unit cell are indicated.

In this work, we address the nucleation, growth and thermal stability of Pt particles on the (√2×√2)R45°-Fe_3O_4(001) surface and compare the results with those previously obtained in our laboratories for the Pt/Fe_3O_4(111) system which exhibits a classical SMSI effect via encapsulation as clearly demonstrated by STM and CO adsorption studies. In contrast to the hemispherical particles obtained for Pt on Fe_3O_4(111), the Pt nanoparticles on Fe_3O_4(001) shown here assume a cuboid shape upon annealing at high temperatures. Nonetheless, the Pt particles become encapsulated by an iron oxide overlayer which is an FeO(111)

monolayer in nature, i.e. in the same manner as on a Fe_3O_4(111) support. The results shed more light on the structure sensitivity of the SMSI effects on Pt-based catalysts.

Results and Discussion

As reported in our previous paper,[17] pristine Fe_3O_4(001) thin films expose wide flat terraces with few screw dislocations. Figure 2a displays a high-resolution STM image showing the atomic rows running in the <110> direction characteristic for the (√2×√2)R45° reconstruction. In addition, defects imaged either as weak depressions or protrusions about 1 Å in depth (height) are frequently observed (see inset in Fig. 2a). Both features are located over the protruding rows which correspond to the octahedral Fe atoms in the topmost layer[10a, 11, 18] (see Fig. 1b). Following Parkinson and co-workers, [10a] we assign ad-species to adventitious hydroxyls formed by the reaction with residual gases in our ultra-high vacuum (UHV) chamber. Accordingly, the depressions could tentatively be attributed to Fe vacancies in the topmost layer.

Figure 2b shows an STM image after deposition of 0.15 ML of Pt at 300 K (one monolayer (ML) of Pt corresponds to one Pt atom per (√2×√2)R45° surface unit cell, i.e. 1.4 x 10^{-14} at/cm^2). Besides the weak OH-protrusions remaining at the surface, two other types of protrusions are observed, which must therefore be attributed to Pt. The majority of the additional protrusions are ~2.5 Å in height and are located between the Fe-rows. These are assigned to single Pt atoms in the same manner as for Pd, Au, and Ag. [10a, 11-12] Again, the registry analysis (Fig. 2c) reveals that the Pt atoms occupy the so-called “narrow” sites on the (√2×√2)R45°-reconstructed Fe_3O_4(001) surface.

Additionally, a few larger protrusions of ~ 6 Å in height and ~ 15 Å in lateral size are observed, which are assigned to Pt clusters. The Pt ad-atoms and clusters are found randomly distributed on the entire oxide surface and show no preferential nucleation on step edges and screw dislocations. This implies a relatively strong interaction of the Pt atoms with the (√2×√2)R45°-Fe_3O_4(001) surface resulting in limited surface diffusion that, in turn, prevents Pt agglomeration into the larger clusters. The formation of Pt clusters in our experiments may also result from adsorption of residual gases (such as CO) as previously shown for Pd ad-atoms.[11]

Basically, such a nucleation-growth mode remains at increasing Pt coverage up to 1 ML, where the surface is mostly covered by Pt ad-atoms, although the density of three-dimensional nanoparticles apparently increases (Fig. 2d). Similar behaviour was previously reported for the Ag ad-atoms.[12] The higher density of nanoparticles observed here for Pt when compared to Ag may be explained by the stronger interaction of Pt ad-atoms with residual gas molecules which, in turn, weaken the Pt bonds to the support. Indeed, Au ad-atoms, as presumably more weakly bound species, showed sintering at considerably lower coverages.[10a]

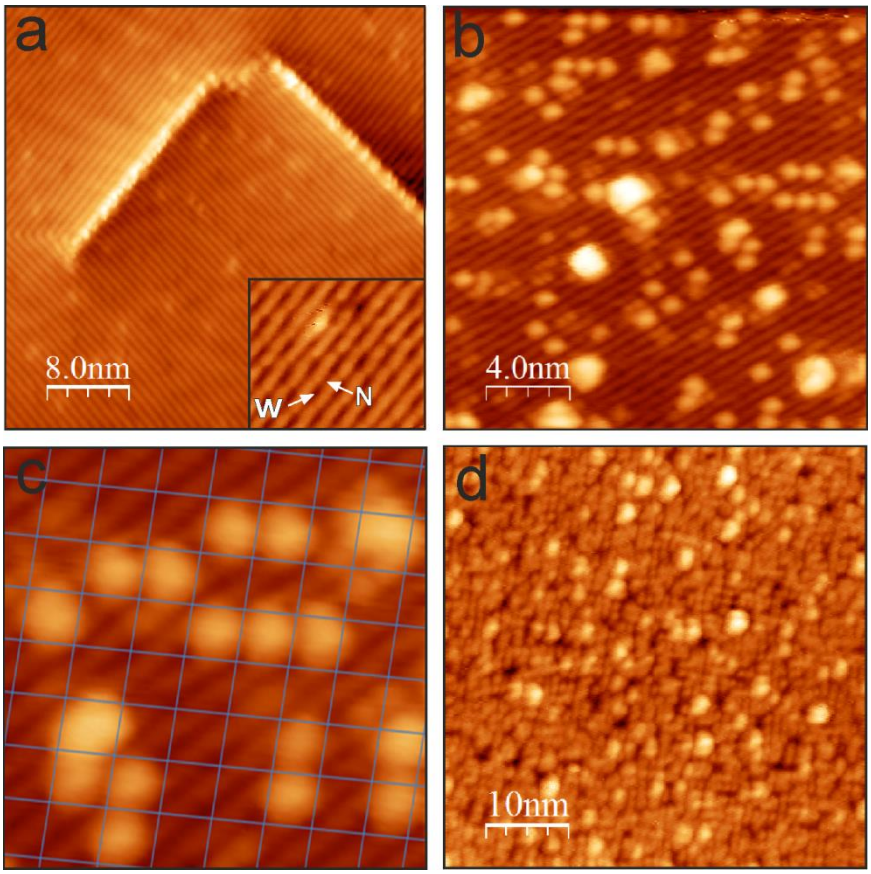

Figure 2. STM images of a clean Fe_3O_4(001) film (a), and after deposition of 0.15 ML (b,c) and 1 ML (d) Pt at 300 K. "Wide" (w) and "narrow" (N) adsorption sites (see Fig. 1b) within the (√2×√2)R45°-Fe_3O_4(001) unit cell are indicated in the inset in panel (a). In panel (c), the lines join the wide sites, therefore the Pt ad-atoms occupy the narrow sites. (Tunneling conditions: (a) bias -1V, current 0.5nA; (b,c) -1V, 0.7nA; (d) -1.5 V, 1 nA).

In the next set of experiments, we examined the thermal stability of the Pt deposits by stepwise annealing in UHV to elevated temperatures. Figure 3 displays a series of STM images obtained for 1 ML Pt/Fe_3O_4(001). Compared to the "as deposited" sample (Fig. 2d),

UHV annealing at 500 K for 10 min does not cause considerable morphological changes (Fig. 3a), albeit the density of clusters increases. Metal sintering only becomes substantial after annealing at 700 K (Fig. 3b). The Pt nanoparticles can clearly be recognized, growing both laterally and in height at the expense of monoatomic species. Further sintering, presumably via Ostwald ripening, proceeds upon heating to 850 K (Fig. 3c). Ultimately, after annealing at 1000 K, Pt nanoparticles with a cuboid shape dominate the surface (Fig. 3d).

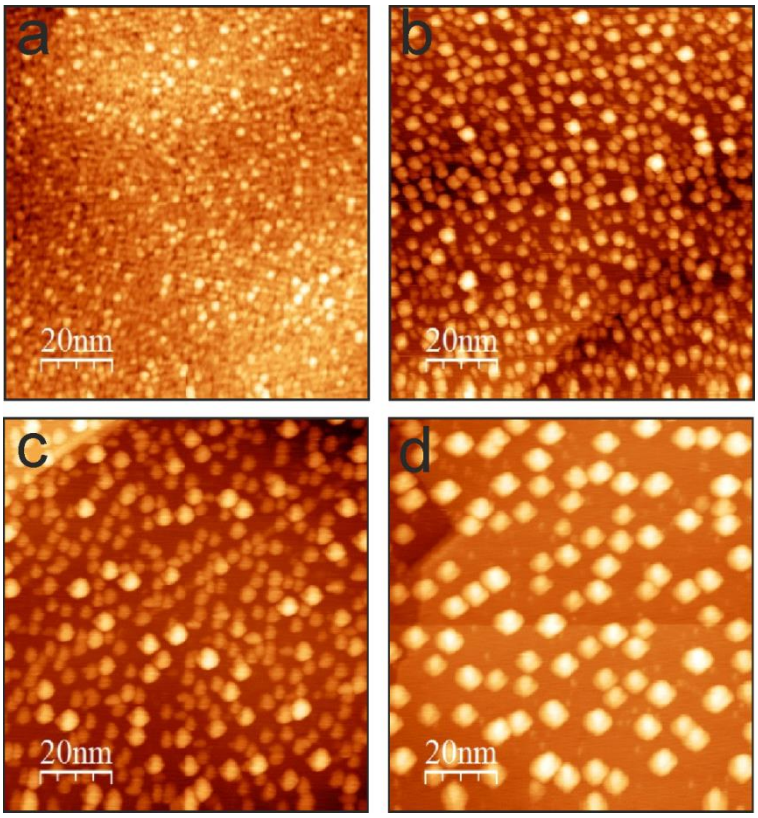

Figure 3. STM images of 1 ML Pt/Fe_3O_4(001) stepwise annealed at 500 K (a), 700 K (b), 850 K (c), and 1000 K (d). (Tunneling conditions: bias -2 V, current 0.7 nA (a,b); -2 V, 1 nA (c,d)).

The high-resolution STM image in Fig. 4a reveals that the edges of the Pt particles are oriented along the Fe-rows on the surrounding (√2×√2)R45°-reconstructed surface of Fe_3O_4(001). Solely on the basis of these STM images, one can envision that Pt grows in the (001) orientation parallel to the (001) plane of Fe_3O_4, i.e. similar to the epitaxial relationships reported in ref. [13] although observed on 2-5 nm-thick Pt films grown on Fe_3O_4(001) at high temperatures. Our previous LEED results for the growth of Fe_3O_4(001) films on a Pt(001) substrate showed that lattice vectors of Pt(001) are oriented along the

lattice vectors of Fe_3O_4(001)-(1×1).[17] It is therefore plausible that the same mutual orientation holds true for the inverse interface, i.e. Pt on an Fe_3O_4(001) substrate. This suggests that the atomic rows on Pt(001) facets run along the Fe-rows on the (√2×√2)R45°-reconstructed Fe_3O_4(001) surface (see Fig. 1b). Based on this and electron microscopy diffraction patterns reported in ref. [13], we can envision a truncated Pt cuboid particle as schematically shown in Fig. 4b.

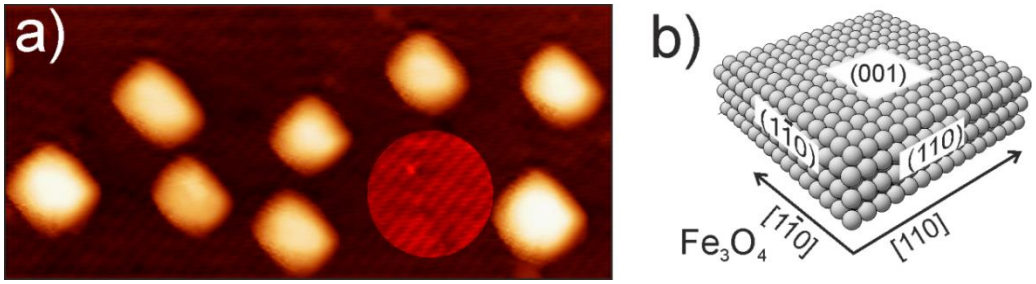

Figure 4. (a) STM image of 1 ML Pt/Fe_3O_4(001) annealed at 1000 K. The atomic rows of the support are highlighted in the circle to show the orientation of the particles with respect to the support. (Tunneling bias -1.5 V, and current 1 nA). (b) Schematic representation of the cuboid Pt particles.

Similar annealing experiments performed on 1.5 and 4 ML Pt samples revealed essentially the same behavior: Sintering sets in at around 700 K, with the progressive formation of the well-shaped Pt nanoparticles at elevated temperatures. For comparison, Figure 5 only shows the morphologies of samples annealed to 1000 K. Again, all annealed particles ultimately showed the cuboid shape. The annealing time needed to reach such a shape is relatively long, i.e. in the range of 30 min. Figure 5b shows that annealing of 1.5 ML Pt sample for 10 min resulted in a mixture of hexagonally- and rectangular-shaped top facets. The latter dominate the surface only after further annealing for 30 min (Fig. 5c). For the highest Pt coverage studied here (i.e. 4 ML), some template effects could be seen in Fig. 5d, as the cuboid Pt particles form quasi-ordered arrays along the crystallographic directions of the support. Interestingly, with increasing Pt coverage, the lateral size of the annealed particles, on average, remains the same, and only the particle density and heights increase.

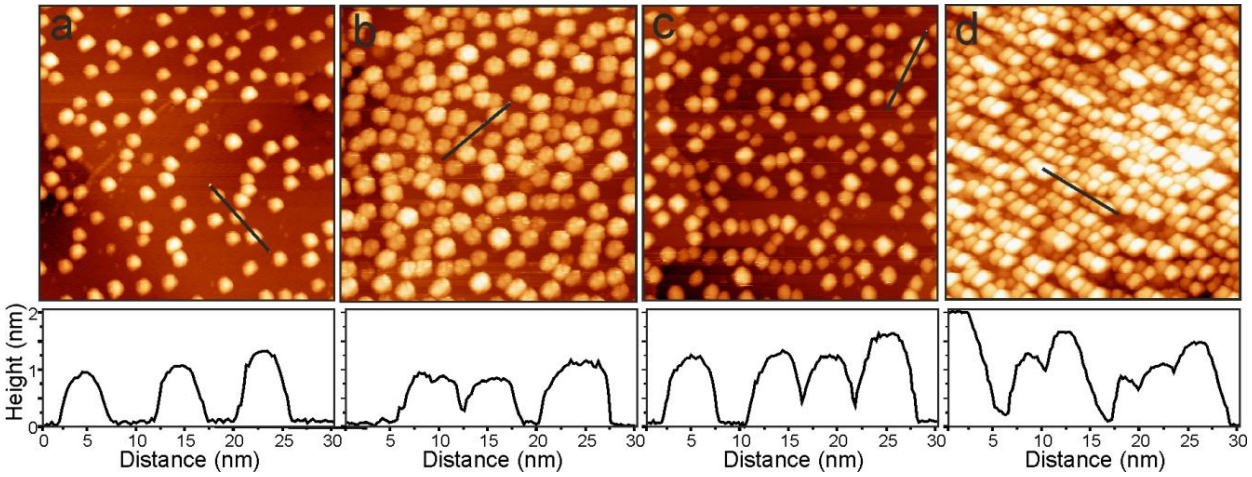

Figure 5. STM images and corresponding profile lines of the $Pt/Fe_3O_4(001)$ samples, all annealed at 1000 K. (a) Pt coverage is 1 ML, and the annealing time is 30 min; (b) 1.5 ML, 10 min; (c) 1.5 ML, 40 min; (d) 4 ML, 30 min. All image sizes are 100 nm x 100 nm. Tunneling conditions: bias -2 V, current 1 nA (a); -1.5 V, 1 nA (b-d).

To address the SMSI effects on high-temperature annealing, we carried out temperature programmed desorption (TPD) experiments using CO as a probe molecule to titrate the Pt surface since the iron oxide support does not adsorb CO at 300 K. CO TPD spectra obtained on the 1.5 ML $Pt/Fe_3O_4(001)$ surface stepwise-annealed to the specified temperatures are shown in Fig. 6a. Structural characterization after each annealing step was performed with STM and LEED.

The "as deposited" $Pt/Fe_3O_4(001)$ surface showed a broad desorption signal between 300 and 520 K with a maximum at 450 K, that falls into the range observed for single crystal Pt surfaces.[19] Note, however, that CO induced sintering of the Pt ad-atoms, as previously observed for $Pd/Fe_3O_4(001)$,[11] might also affect the first TPD spectrum. Annealing at 600 K slightly (by ~ 15 %) reduces the CO uptake, and several desorption features at 360, 420 and 450 K can be resolved. These features remain after annealing at 700 K, which further reduces the CO uptake. The latter drops to almost zero upon annealing to 850 K, although Pt particles did not show considerable sintering (see Figure S1 in the Supporting Information), thus providing direct evidence that the Pt particles exhibit the SMSI effect at elevated temperatures most likely via encapsulation. Indeed, the formation of Pt-Fe alloys as another option to explain the CO uptake drop would manifest itself as a prominent desorption signal at around 300 K [20] which is not the case here. Ultimately, annealing at 1000 K totally suppresses CO adsorption and it is accompanied by reshaping of the Pt particles.

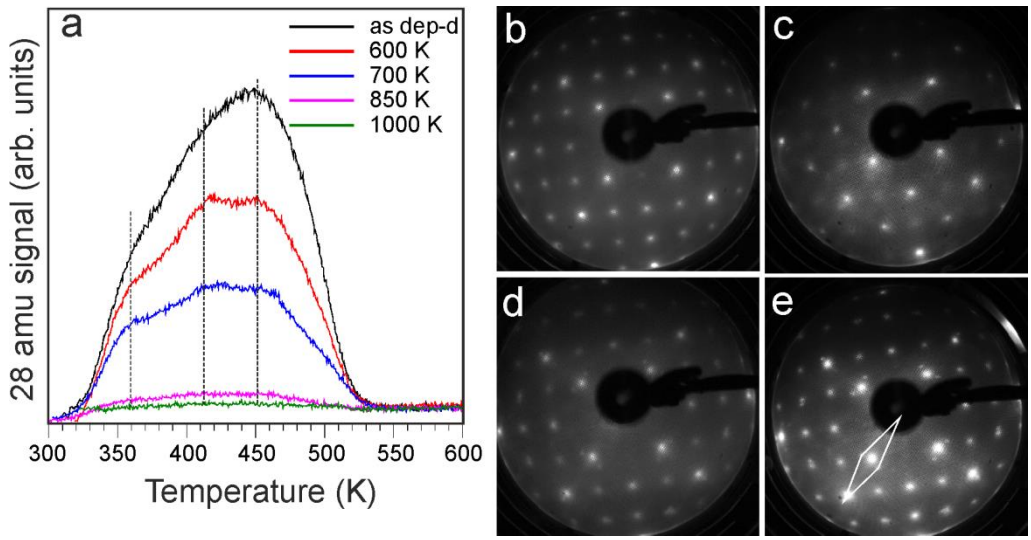

Figure 6. (a) TPD spectra of 20 L CO adsorbed at 300 K on 1.5 ML Pt/Fe_3O_4(001) as deposited at 300 K and then UHV annealed to the indicated temperature. The heating rate is 2 K/s. (b-e) LEED patterns (at 95 eV) of the pristine (√2×√2)R45°-Fe_3O_4(001) surface (b); after deposition 1.5 ML of Pt at 300 K (c); and subsequent UHV annealing to 850 K for 10 min (d) and 1000 K for 30 min (e), respectively. The additional spots are developed, which are assigned to FeO(111)/Pt(001)-c(2x10) structure as marked in the panel (e).

LEED patterns of the same Pt/Fe_3O_4(001) surfaces recorded before the TPD runs are shown in Fig. 6(b-d). Additional diffraction spots (marked in Fig. 6e) appear upon annealing which were absent on the pristine Fe_3O_4(001) film annealed at the same temperature (1000 K) prior to the Pt deposition. These spots first develop upon heating to 850 K and become more intense and sharper by annealing at 1000 K. The corresponding surface structure is virtually identical to that observed for an ultrathin iron oxide film grown on a Pt(100) single crystal and assigned to an FeO(111)/Pt(100)-c(2x10) (and/or –(2x9)) coincidence structure.[21] Bearing in mind the cuboid morphology of the annealed Pt nanoparticles which preferentially expose the top (100) facets (Fig. 4b), the LEED observation of the FeO(111)/Pt(100) interface can readily be explained by the encapsulation of the Pt particles by an FeO(111) layer. One could argue, however, that the new ordered structure arises from the interface underneath rather than on the top of a Pt particle, although the spots seem to be too bright to make the former assignment.

To shed more light on this issue, we have performed sputtering experiments as follows. The 1.5 ML Pt sample annealed to 1000 K was subjected to a mild Ar^+-ion bombardment (500 eV, ~1 μA/cm^2, 45° incidence, for 10 sec) at room temperature.

Certainly, this treatment caused some surface roughening as judged by STM (Fig. 7a). However, the atomic rows of the (√2×√2)R45°-reconstructed Fe_3O_4(001) between the particles are still visible as shown in Fig. 7c, thus indicating that ion bombardment at our conditions does not cause severe sputtering, but creates surface defects. However, the FeO(111)/Pt(100) diffraction spots fully disappear (inset in Fig. 7a). Moreover, CO start to adsorb on the sputtered surface as observed by TPD (Fig. 7e), indicating that the ion sputtering removed the encapsulating layer and exposed the Pt surface.

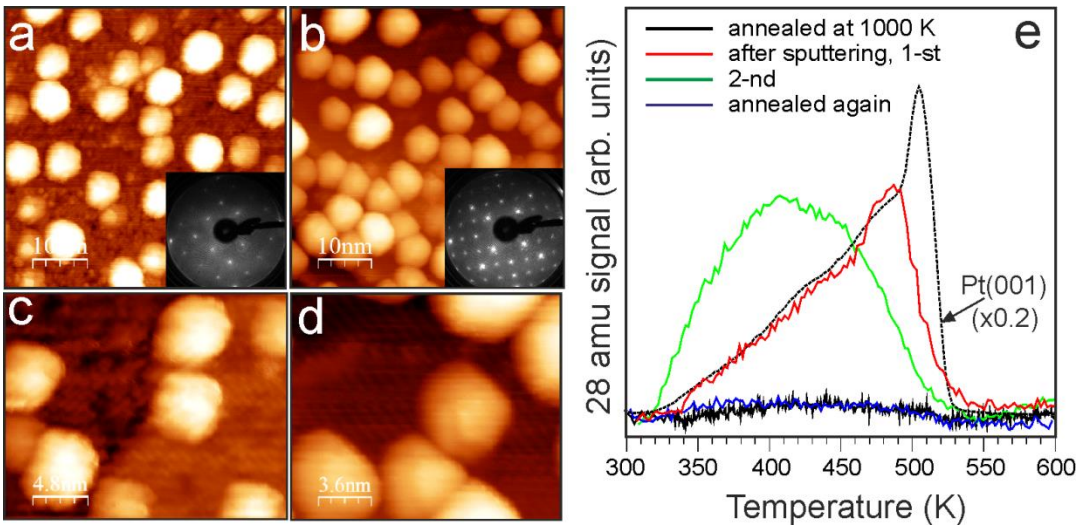

Figure 7. (a-d) STM images and corresponding LEED patterns (at 95 eV in insets) of 1.5 ML Pt/Fe_3O_4(001) annealed at 1000 K for 30 min and then Ar^+- ion sputtered at 300 K (a,c); and re-annealed at 1000 K for 10 min (b,d). (Tunneling conditions for all images are bias -1.5 V, and current 1 nA). (e) TPD spectra of 20 L CO adsorbed at 300 K on the same samples as indicated. The heating rate is 2 Ks^{-1}. The spectrum on the clean, hex-reconstructed Pt(001) surface, taken prior to the growth of the Fe_3O_4(001) film, is shown as dashed line for comparison.

Interstingly, the first CO TPD spectrum revealed a prominent peak at ~ 500 K that show similarities to the spectrum measured on the clean hex-Pt(001) surface. It is tempting to assign this feature to the top (100) facets of the Pt particles opened upon ion sputtering of the encapsulated layer. However, such a TPD profile can also be associated with highly stepped Pt surfaces [19] and, more generally, to the low-coordinated Pt atoms formed on the Pt particles upon sputtering of the Pt surface beyond the encapsulating layer. Indeed, the second CO TPD run already showed a broad signal similar to the one measured on "as prepared" Pt particles (Fig. 6a). Re-annealing of the sample at 1000 K for 10 min, in essence,

recovers the initial characterisitcs of the sample prior to the treatment: The FeO(111)/Pt(100) difraction spots reappear, and the CO uptake drops back to zero.

Therefore, the above-presented LEED, STM and TPD results provide strong evidence that Pt nanoparticles undergo the SMSI effect via encapsulation by an iron oxide layer which is an FeO(111) monolayer in nature. Unfortunately, atomic resolution of the Pt particles could not be achieved with our microscope (basically, because of their small size), which would otherwise allow us to determine the atomic structure of the Pt top facets more precisely.

Nonetheless, we are now in the position to compare the structural properties of Pt/Fe_3O_4(001) and Pt/Fe_3O_4(111) systems [3b, 3c, 8] using thin film supports grown on Pt(100) and Pt(111) substrates, respectively. On both the (001) and (111) magnetite surfaces, Pt shows no preferential nucleation on defects and appears uniformly dispersed across the entire surface. Pt on the (√2×√2)R45°-Fe_3O_4(001) surface adsorbs monoatomically even at 300 K, occupying the "narrow" sites. On Fe_3O_4(111), the adsorption sites for Pt were not yet determined, since STM imaging at low Pt coverages is obscured by the presence of poorly defined adsorbate-like species.[14a, 22] Since DFT predicts strong adsorption of Pt on Fe_3O_4(111) (i.e. ~ 2.2 eV on the Fe-terminated surface),[23] one could envision the monoatomic Pt adsorption on Fe_3O_4(111) as well. Indeed, STM images of Pt/Fe_3O_4(111) at sub-monolayer coverages revealed high density of small islands, which are only about 2 Å in height, corresponding to a single Pt layer.[3c] At increasing coverage, the monolayer islands coalesce and form an extended, irregularly shaped network, and only a few Pt particles two layers in height are observed at 300 K. Therefore, for both Fe_3O_4(100) and (111) surfaces, Pt strongly interacts with magnetite, leading, in essence, to Pt wetting the oxide surface at room temperature.

For both systems, high-temperature annealing in UHV causes Pt sintering and subsequent formation of well-faceted three-dimensional nanoparticles with their edge at the interface running along the crystallographic directions of the oxide surface. These particles exhibit an octahedral shape on Fe_3O_4(111), but a cuboid shape on Fe_3O_4(001), following the epitaxial relationships between Pt and Fe_3O_4, i.e. Pt(111)[1−10]//Fe_3O_4(111)[1−10][24] and Pt(001)[100]//Fe_3O_4(001)[100],[13] thus resulting in the particles exposing Pt(111) and Pt(001) top facets on Fe_3O_4(111) and Fe_3O_4(001), respectively. A difference one would mention is that Pt particles on Fe_3O_4(111) remarkably

coalesce and form extended Pt islands,[3c, 8] whereas Pt on Fe_3O_4(001) forms individual particles about 5 nm in lateral size, at most. This finding could be indicative of the difference in adhesion energy and linked to the stress deformations on the two interfaces as a result of the mismatch between the two lattices. As another factor, we note our high resolution electron microscopy studies of encapsulated Pt/Fe_3O_4(111) particles which showed Fe enrichment of the interface between a Pt particle and an underlying support that results in more Pt-Fe bonds. As the Fe_3O_4(001) surface is initially terminated both by Fe and O atoms, it may well be that limited lateral growth of the Pt particles on Fe_3O_4(001) along the interface may be linked to the interface structure which cannot be addressed with tools employed in the present study.

Conclusions

In this work, we studied nucleation, growth and thermal stability of Pt deposited on the (√2×√2)R45° reconstructed surface of Fe_3O_4(001) thin films. At low and medium coverages, Pt preferentially adsorbs monoatomically on the so-called "narrow" sites, i.e. in the same manner as previously reported for Ag, Pd and Au ad-atoms supported on a Fe_3O_4(001) single crystal. Vacuum annealing above 700 K leads to Pt sintering and concomitantly to re-shaping (at ~1000 K) into cuboid Pt nanoparticles, with edges oriented along the crystallographic directions of the Fe_3O_4(001) surface. In addition, high-temperature annealing suppresses CO adsorption on Pt, thus manifesting a SMSI effect via Pt encapsulation by the oxide support. The combined LEED, STM and TPD results provide strong evidence for the encapsulating overlayer to be identified as FeO(111) as previously observed for a FeO monolayer film on a Pt(001) single crystal. The results are compared with the Pt/Fe_3O_4(111) system, showing the encapsulation of (111)-oriented, hemispherical Pt nanoparticles by the FeO(111) layer. The comparison of two systems suggests that the SMSI effect via encapsulation is insensitive to the surface structure of oxide, although the latter strongly affects the particle morphology.

Experimental Section

The experiments were performed in an UHV chamber (base pressure 2×10^{-10} mbar) equipped with LEED and Auger electron spectroscopy (from Specs), STM (Omicron) and a differentially pumped quadrupole mass spectrometer (QMS, Hiden 201) for TPD

measurements. The Pt(001) crystal (99.95%, from MaTeck) was mounted on the Omicron sample holder and could be heated by electron bombardment from the backside of the crystal using a tungsten filament. The temperature was measured with a chromel-alumel thermocouple spot-welded to the edge of the crystal. The crystal temperature and the heating rate were precisely controlled using a feedback system.

The Fe_3O_4(001) film was grown on a Pt(001) substrate as described in detail in ref. [17]. Briefly, about 3 nm Fe was evaporated onto the clean, hex-reconstructed Pt(001) surface at 300 K as a buffer layer and subsequently 3 nm Fe was deposited with O_2 background pressure of 5×10^{-6} mbar at 300 K. The sample was then UHV-annealed at 1020 K for 10 min. The quality of the prepared films was each time inspected by STM. Prior to the Pt deposition, the Fe_3O_4(001) film was flashed to 600 K to desorb adventitious adsorbates.

Iron and platinum (both 99.95%, Goodfellow) were deposited using commercial e-beam assisted evaporators (Focus EFM3). During Pt deposition, the sample was biased with a retarding potential to prevent metal ions from being accelerated towards the sample. The STM images were obtained at 300 K with commercial Pt-Ir tips (LOT Oriel GmbH).

Acknowledgements

The work was supported by Fonds der Chemischen Industrie and German Science Foundation through Cluster of Excellence UNICAT administered by TU Berlin, and SFB 1109 administered by HU Berlin. The authors acknowledge COST Action CM1104.

References

[1] S. J. Tauster, *Acc. Chem. Res.* **1987**, *20*, 389-394.

[2] a) J. Liu, *ChemCatChem* **2011**, *3*, 934-948; b) S. Penner, D. Wang, D. S. Su, G. Rupprechter, R. Podloucky, R. Schlögl, K. Hayek, *Surf. Sci.* **2003**, *532–535*, 276-280; c) S. Bernal, J. J. Calvino, M. A. Cauqui, J. M. Gatica, C. Larese, J. A. Pérez Omil, J. M. Pintado, *Catal. Today* **1999**, *50*, 175-206.

[3] a) O. Dulub, W. Hebenstreit, U. Diebold, *Phys. Rev. Lett.* **2000**, *84*, 3646-3649; b) Z. H. Qin, M. Lewandowski, Y. N. Sun, S. Shaikhutdinov, H. J. Freund, *J. Phys. Chem. C* **2008**, *112*, 10209-10213; c) Z. H. Qin, M. Lewandowski, Y. N. Sun, S. Shaikhutdinov, H. J. Freund, *J. Phys.-Condes. Matter* **2009**, *21*; d) M. Bowker, P. Stone, P. Morrall, R. Smith, R. Bennett, N. Perkins, R. Kvon, C. Pang, E. Fourre, M. Hall, *J. Catal.* **2005**, *234*, 172-181.

[4] T. Suzuki, R. Souda, *Surf. Sci.* **2000**, *448*, 33-39.

[5] M. G. Willinger, W. Zhang, O. Bondarchuk, S. Shaikhutdinov, H.-J. Freund, R. Schlögl, *Angew. Chem. Intern. Ed.* **2014**, *53*, 5998-6001.

[6] a) C. Kuhrs, Y. Arita, W. Weiss, W. Ranke, R. Schlögl, *Top. Catal.* **2000**, *14*, 111-123; b) Y. Joseph, W. Ranke, W. Weiss, *J. Phys. Chem. B* **2000**, *104*, 3224-3236; c) S. K. Shaikhutdinov, W. Weiss, R. Schlögl, *Appl. Surf. Sci.* **2000**, *161*, 497-507; d) W. Weiss, W. Ranke, *Progr. Surf.*

Sci. **2002**, *70*, 1-151; e) R. S. Cutting, C. A. Muryn, G. Thornton, D. J. Vaughan, *Geochim. Cosmochim. Acta* **2006**, *70*, 3593-3612.
[7] a) R. Meyer, K. Shaikhutdinov Sh, H. J. Freund, *Z. Phys. Chem.* **2004**, *218*, 905; b) S. K. Shaikhutdinov, R. Meyer, M. Naschitzki, M. Bäumer, H. J. Freund, *Catal. Lett.* **2003**, *86*, 211-219.
[8] M. Lewandowski, Y. N. Sun, Z. H. Qin, S. Shaikhutdinov, H. J. Freund, *Appl. Catal. A* **2011**, *391*, 407-410.
[9] a) T. Kendelewicz, P. Liu, C. S. Doyle, G. E. Brown Jr, E. J. Nelson, S. A. Chambers, *Surf. Sci.* **2000**, *453*, 32-46; b) G. S. Parkinson, Z. Novotný, P. Jacobson, M. Schmid, U. Diebold, *J. Amer. Chem. Soc.* **2011**, *133*, 12650-12655.
[10] a) Z. Novotný, G. Argentero, Z. Wang, M. Schmid, U. Diebold, G. S. Parkinson, *Phys. Rev. Lett.* **2012**, *108*, 216103; b) N. Spiridis, E. Madej, J. Korecki, *J. Phys. Chem. C* **2014**, *118*, 2011-2017; c) K. Jordan, S. Murphy, I. V. Shvets, *Surf. Sci.* **2006**, *600*, 5150-5157.
[11] G. S. Parkinson, Z. Novotny, G. Argentero, M. Schmid, J. Pavelec, R. Kosak, P. Blaha, U. Diebold, *Nat. Mater.* **2013**, *12*, 724-728.
[12] R. Bliem, R. Kosak, L. Perneczky, Z. Novotny, O. Gamba, D. Fobes, Z. Mao, M. Schmid, P. Blaha, U. Diebold, G. S. Parkinson, *ACS Nano* **2014**, *8*, 7531-7537.
[13] C. Gatel, E. Snoeck, *Surf. Sci.* **2006**, *600*, 2650-2662.
[14] a) A. Sala, H. Marchetto, Z. H. Qin, S. Shaikhutdinov, T. Schmidt, H. J. Freund, *Phys. Rev. B* **2012**, *86*, 155430; b) A. R. Lennie, N. G. Condon, F. M. Leibsle, P. W. Murray, G. Thornton, D. J. Vaughan, *Phys. Rev. B* **1996**, *53*, 10244-10253.
[15] a) R. Pentcheva, F. Wendler, H. L. Meyerheim, W. Moritz, N. Jedrecy, M. Scheffler, *Phys. Rev. Lett.* **2005**, *94*, 126101; b) Z. Łodziana, *Phys. Rev. Lett.* **2007**, *99*, 206402.
[16] R. Bliem, E. McDermott, P. Ferstl, M. Setvin, O. Gamba, J. Pavelec, M. A. Schneider, M. Schmid, U. Diebold, P. Blaha, L. Hammer, G. S. Parkinson, *Science* **2014**, *346*, 1215-1218.
[17] E. M. Davis, K. Zhang, Y. Cui, H. Kuhlenbeck, S. Shaikhutdinov, H.-J. Freund, *Surf. Sci.* **2015**, *636*, 42-46.
[18] G. S. Parkinson, Z. Novotný, P. Jacobson, M. Schmid, U. Diebold, *Surf. Sci.* **2011**, *605*, L42-L45.
[19] R. W. McCabe, L. D. Schmidt, *Surf. Sci.* **1977**, *66*, 101-124.
[20] Y. N. Sun, Z. H. Qin, M. Lewandowski, S. Shaikhutdinov, H. J. Freund, *Surf. Sci.* **2009**, *603*, 3099-3103.
[21] a) S. Shaikhutdinov, M. Ritter, W. Weiss, *Phys. Rev. B* **2000**, *62*, 7535-7541; b) G. H. Vurens, V. Maurice, M. Salmeron, G. A. Somorjai, *Surf. Sci.* **1992**, *268*, 170-178; c) M. Ritter, H. Over, W. Weiss, *Surf. Sci.* **1997**, *371*, 245-254.
[22] a) C. Lemire, R. Meyer, V. E. Henrich, S. Shaikhutdinov, H. J. Freund, *Surf. Sci.* **2004**, *572*, 103-114; b) S. Shaikhutdinov, W. Weiss, *J. Mol. Catal. A* **2000**, *158*, 129-133.
[23] X. Yu, X. Tian, S. Wang, *Surf. Sci.* **2014**, *628*, 141-147.
[24] C. Gatel, E. Snoeck, *Surface Science* **2007**, *601*, 1031-1039.

TOC graphic.

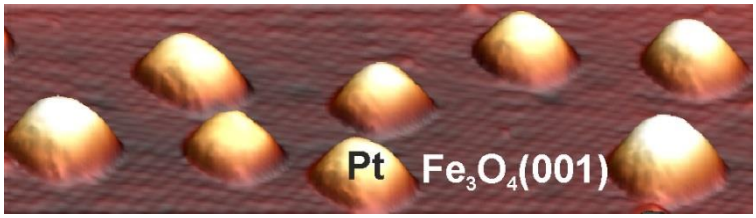

Platinum deposited on the (√2×√2)R45° reconstructed surface of Fe_3O_4(001) thin films exhibits a strong metal-support interaction resulting in cuboid Pt nanoparticles, with edges oriented along the crystallographic directions of the Fe_3O_4(001) surface, encapsulated by an FeO(111) single layer, i.e. in the same manner as previously observed for hemispherical Pt particles on a Fe_3O_4(111) support. The results shed light on the structural sensitivity of the SMSI effects.